World Journal of Engineering Research
Print ISSN: 2959-9865
Online ISSN: 2959-9873
DOI: https://doi.org/10.61784/wjer3077

IDENTIFICATION OF A CRITICAL INITIAL TEMPERATURE WINDOW FOR PEMFC COLD START UNDER LINEAR 25 S LOADING BASED ON A ONE-DIMENSIONAL MULTIPHASE MODEL

YueWen Zeng*, Lei Shi
College of Automotive and Energy Engineering, Tongji University, Shanghai 201804, China.
**Corresponding Author: YueWen Zeng*

Abstract: The low-temperature cold-start capability of proton exchange membrane fuel cells (PEMFCs) is strongly influenced by the initial temperature and the water-thermal coupling behavior within the stack. In this study, a one-dimensional multiphase cold-start model was developed based on a lumped-parameter approach. A 5 kW stack consisting of 30 single cells was investigated under a unified linear 25 s loading strategy, in which the current density was linearly increased from 0 to 0.5 $A \cdot cm^{-2}$ and then maintained constant. The cold-start evolution characteristics were systematically analyzed over an initial temperature range from -4 °C to -20 °C. The simulation results reveal the existence of a distinct critical initial temperature interval (approximately -12 °C to -14 °C) under the prescribed loading protocol, with the upper and lower bounds corresponding to two fundamentally different evolutionary pathways. When the initial temperature exceeds the lower bound of this interval, the stack establishes a stable positive thermo-electrical coupling feedback, enabling voltage recovery and sustained operation. In contrast, when the initial temperature falls below this interval, the system progressively enters an irreversible degradation trajectory and ultimately becomes unstable. Further analysis indicates that the decisive factor governing cold-start success is not the overall heat generation level, but whether the edge cells can surpass the freezing point and complete ice melting within a critical time window. These findings provide a theoretical basis for cold-start boundary identification and strategy optimization.
Keywords: PEMFC; Cold start; Cold start temperature; Voltage consistency; Numerical simulation

1 INTRODUCTION

Low-temperature cold-start performance and cell-to-cell consistency are critical indicators for the reliable operation of proton exchange membrane fuel cells (PEMFCs). They directly determine the adaptability and durability of PEMFC systems in subzero environments and remain one of the key bottlenecks restricting large-scale commercialization [1]. Driven by the “dual-carbon” strategy, PEMFCs have attracted increasing attention as highly efficient and zero-emission power sources. However, the challenges associated with low-temperature cold start have become increasingly prominent. Variations in the initial startup temperature can significantly affect startup reliability and operational stability. During the cold-start process, water generated by electrochemical reactions readily condenses and freezes inside the cell. The startup temperature influences water transport, phase transition, and ice formation, thereby affecting proton conduction, gas diffusion, and electrochemical reaction kinetics. Consequently, it directly governs the smoothness of the cold-start process and the consistency between successive cycles[2-3].

Existing studies have demonstrated significant differences in cold-start performance under varying startup temperatures. Lower temperatures intensify internal ice formation, block gas diffusion pathways, cover active sites in the catalyst layer, and increase electrical contact resistance, ultimately leading to startup failure or performance degradation [4-5]. Due to the high cost and experimental complexity associated with fuel cell cold-start testing, numerical simulation has become an essential tool for investigating low-temperature startup behavior. Although extensive simulation studies have been conducted worldwide, clarifying the relationships among ambient temperature, freezing characteristics, water transport and phase transition, and output performance [6-8], quantitative investigations into the coupling between startup temperature, cold-start performance, and cell-to-cell consistency remain insufficient.

Motivated by these considerations, this study focuses on the numerical investigation of PEMFC cold-start behavior under different subzero startup temperatures. A detailed simulation framework is employed to analyze water–thermal transport, phase transition and ice formation, as well as electrochemical characteristics under varying temperature conditions. The influence of startup temperature on cold-start performance (including startup time, success rate, and output characteristics) and consistency (including parameter fluctuation and reaction stability) is systematically examined. The findings provide theoretical support and simulation-based guidance for optimizing PEMFC cold-start control strategies and enhancing system adaptability under extreme low-temperature conditions.

2 ONE-DIMENSIONAL MULTI-PHASE COLD START STACK MODEL AND SIMULATION SETTINGS

The fuel cell stack consists of multiple single cells connected in series and mechanically clamped into an integrated structure by current collectors, insulating plates, and end plates. Each single cell is composed of multiple functional

layers, as illustrated in Figure 1. Specifically, a single cell sequentially includes the proton exchange membrane (MEM), anode and cathode catalyst layers (CLs), anode and cathode gas diffusion layers (GDLs), anode and cathode gas flow channel layers, and anode and cathode coolant channel layers, forming a total of nine major functional layers. These layers are separated by sealing gaskets to prevent cross-permeation of reactant gases and liquid water.

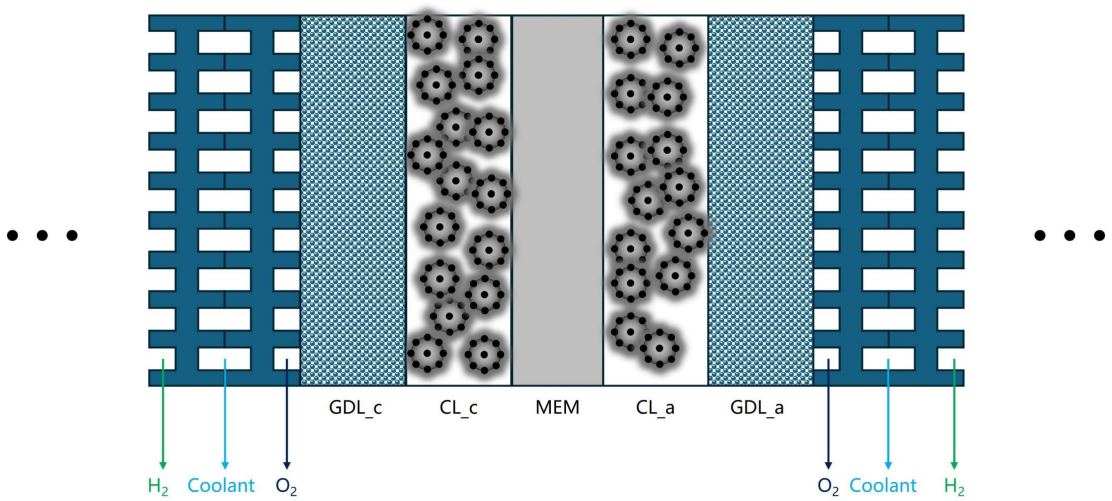

Figure 1 Schematic Diagram of the Layered Structure of a Fuel Cell Single Cell

The cold-start process of a fuel cell is a complex water–thermal transport phenomenon. In addition to the well-known electrochemical reactions, it involves intricate phase-change processes. Water generation, diffusion, and phase transition play decisive roles during low-temperature cold start. Due to differences in material properties and temperature distribution among the layers, water exists in different forms and undergoes dynamic transformations across various regions. Under subzero conditions, five primary forms of water are considered in the fuel cell system: membrane-bound non-frozen water, membrane-bound frozen water, water vapor, ice, and liquid water.

To establish a one-dimensional multiphase cold-start model, it is necessary to comprehensively account for the conservation equations associated with electrochemical reactions (including mass, momentum, species, and charge conservation), as well as the governing equations describing water phase transitions among supercooled liquid water, ice, dissolved water in the membrane, and frozen water in the membrane.

In this study, the low-temperature cold-start model is developed based on a lumped-parameter approach. Each functional layer of a single cell is treated as an independent control volume, and the primary physical variables (such as temperature, species concentration, and water content) are assumed to be uniformly distributed within each control volume and represented by their center values. For each control volume, water–thermal balance equations and phase-transition equations are established, and energy and mass transfer between adjacent layers are solved along the direction perpendicular to the membrane (i.e., the principal transport direction). This approach ensures high computational efficiency while reasonably capturing the multiphysics coupling behavior inside the fuel cell during cold start. The detailed model formulation and validation procedures have been reported in our previous work and are therefore not repeated here [9].

The present study investigates the cold-start process of the fuel cell system under different initial startup temperatures, with particular emphasis on the evolution of stack output performance and voltage consistency during low-temperature operation. The cold-start stack model is based on a 5 kW stack consisting of 30 single cells, each with an effective reaction area of 270 cm^2. The key parameters are listed in Table 1. A unified linear 25 s loading strategy is adopted, in which the current density is linearly increased from 0 to 0.5 $A \cdot cm^{-2}$ within 25 s and then maintained constant. The coolant flow rate is set to 1 $L \cdot min^{-1}$, and the initial membrane water content is 2.4. All other model parameters are consistent with those listed in Table 1. Based on these conditions, cold-start simulations are conducted over an initial temperature range from -4 °C to -20 °C.

Table 1 5 kW Stack Parameters

Parameters/units	Value
Number of cells	30
Effective area/cm^2	270
Rated Power /kW	3.4
Maximum Power /kW	4.2
Anode CL porosity	0.5
Anode CL thickness/mm	0.01
Anode GDL porosity	0.78
Anode GDL thickness/mm	0.17
Cathode CL porosity	0.5
Cathode CL thickness/mm	0.005

Cathode GDL porosity	0.78
Cathode GDL thickness/mm	0.17
Inlet/Outlet Manifold Diameter /mm	32
Inlet/Outlet Manifold Length /m	0.15
Outlet pipe diameter /mm	32
Outlet pipe length /m	1.5
Coolant density /kg·m⁻³	1071

3 RESULTS AND DISCUSSION

To quantitatively evaluate stack consistency during the cold-start process, the voltage fluctuation rate C_V [10] is introduced to characterize the uniformity of single-cell voltage distribution. Its calculation is defined in Eq.(1):

$$C_v = \frac{\text{sd}}{\text{mean}} \times 100\% \tag{1}$$

where *sd* denotes the standard deviation of single-cell voltages and *mean* represents their average value.

Figure 2 (a)–(d) present the dynamic evolutions of stack voltage, average stack temperature, voltage fluctuation rate C_V, and the ice volume fraction in the cathode catalyst layer (CL) of the edge cell (cell-1), respectively. Solid lines correspond to successful cold start (-4 °C to -12 °C), whereas dashed lines represent failed cold start (-14 °C and below). The detailed analysis is as follows.

As shown in Figure 2 (a), the stack voltage exhibits a distinct multi-stage response during low-temperature cold start. In the initial stage (0–10 s), all operating conditions experience a pronounced voltage drop due to the combined increase in activation and ohmic polarization losses under subzero conditions. The lower the initial temperature, the larger the voltage decline. After 10 s, the evolution trends gradually diverge. For the successful cases (-4 °C to -12 °C), the stack voltage progressively recovers as the temperature rises, and a higher initial temperature results in a faster recovery rate. In contrast, for the failed cases (-14 °C to -20 °C), the voltage continues to decrease slowly, with a more severe downward trend at lower temperatures. At t = 25 s, all curves exhibit an inflection point with accelerated voltage increase, directly associated with the current density reaching 0.5 A·cm⁻² and entering the constant-current stage during linear loading. However, while the successful cases achieve sustained and stable voltage recovery after this point, the failed cases show only a brief rebound. Subsequently, the continuous accumulation of ice in the cathode CL of edge cells (e.g., cell-1) severely blocks mass transport pathways, causing rapid voltage decay or even voltage collapse in the edge cells, ultimately leading to significant stack voltage deterioration.

Figure 2 (b) shows that, owing to the identical loading strategy, the overall rising trend of the average stack temperature is similar under all conditions, gradually approaching 0 °C from the initial subzero temperature. Notably, however, certain cases (e.g., -14 °C and -16 °C) still result in cold-start failure even when the average stack temperature exceeds 0 °C. This phenomenon indicates that the average stack temperature cannot fully represent the actual thermal state of individual cells. Due to strong heat dissipation from the metallic end plates, edge cells (e.g., cell-1) exhibit significantly lower temperatures than central cells (e.g., cell-15). Even when the overall stack temperature approaches or surpasses the freezing point, the edge-cell temperature may remain below 0 °C, preventing ice melting and leading to persistent accumulation of mass transport resistance and polarization losses, which ultimately triggers startup failure. Therefore, "overall temperature recovery accompanied by significant cell-to-cell temperature disparity" constitutes an important underlying cause of low-temperature cold-start failure.

As illustrated in Figure 2 (c), the dynamic evolution of the voltage fluctuation rate C_V is strongly coupled with ice formation and inter-cell voltage deviation. During the early stage (0–25 s), all cases exhibit similar trends, characterized by a distinct peak resulting from initial temperature differences among cells. The peak value increases with decreasing initial temperature (e.g., approximately 3.68% at -10 °C and 11.58% at -20 °C). After 25 s, the behaviors clearly diverge. In the successful cases, as ice gradually melts and voltage deviations among cells diminish, C_V rapidly decreases and stabilizes below 5%. In contrast, in the failed cases, following a brief decline, continuous ice accumulation in edge cells leads to substantial voltage decay or collapse, sharply enlarging the deviation from the mean voltage. Consequently, C_V rises dramatically (exceeding 30% in the -20 °C case), indicating a complete loss of voltage uniformity within the stack. Figure 2 (d) further elucidates the distinct cold-start outcomes from the perspective of microscopic phase transition. For the -4 °C and -6 °C cases, no significant ice formation occurs throughout the cold-start process due to the relatively high initial temperature. For the -8 °C, -10 °C, and -12 °C cases, the ice volume fraction in the cathode CL of the edge cell exhibits a "rise-then-fall" pattern: it increases while the temperature remains below freezing, reaches a peak, and then rapidly decreases to zero once the temperature surpasses 0 °C. A higher initial temperature results in a lower peak ice fraction and faster melting. In contrast, for the failed cases (-14 °C to -20 °C), the ice volume fraction increases monotonically and gradually approaches unity without noticeable decline, indicating that the edge-cell temperature never exceeds the freezing point and that generated water continuously accumulates in the form of ice. The high ice fraction completely blocks cathode mass transport channels, causing edge-cell voltage collapse and ultimately resulting in stack voltage deterioration and a sharp increase in C_V.

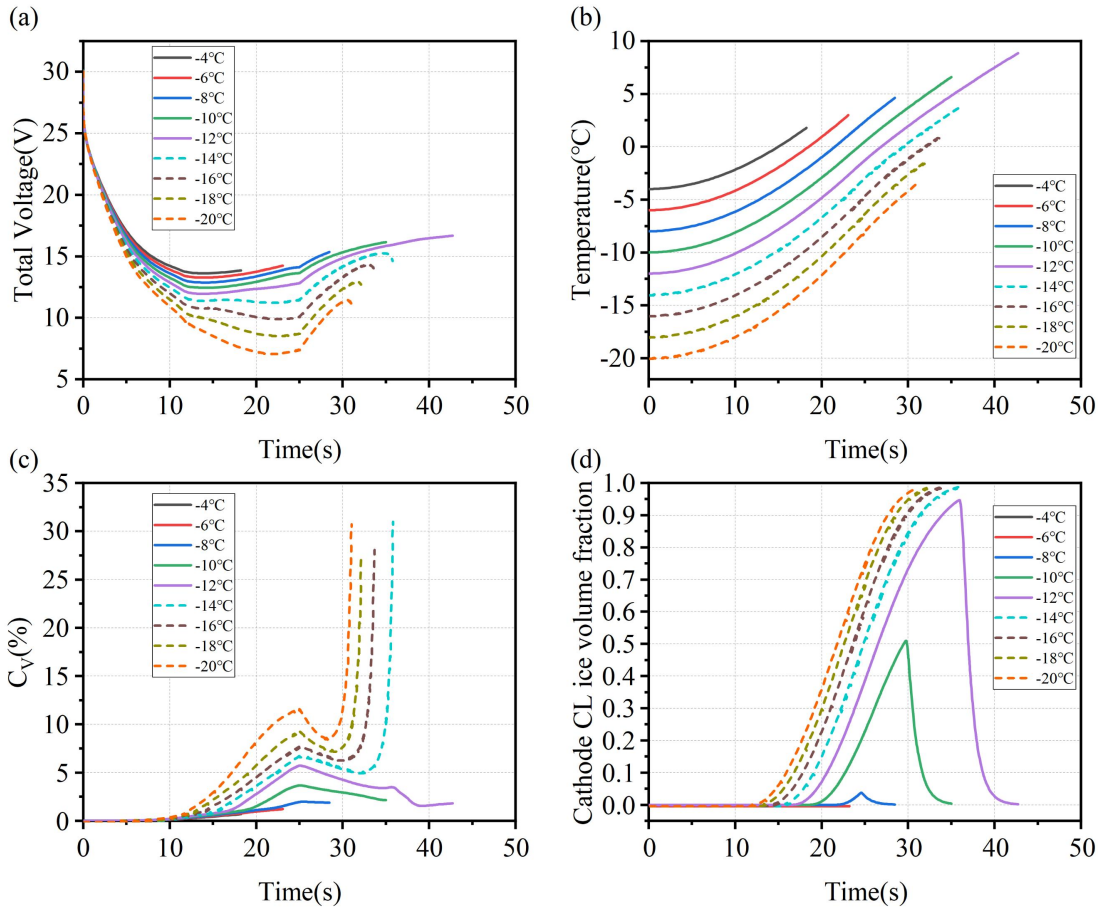

Figure 2 Changes in Total Voltage, Temperature, C_V, and the Volume Fraction of CL Ice in Cell-1 Cathode over Time at Different Starting Temperatures

Under the linear 25 s loading strategy, -12 °C represents the lower temperature limit for successful cold start, whereas -14 °C is identified as the critical temperature below which cold start fails. Figure 3 (a)–(f) illustrate the dynamic evolutions of voltage, cathode catalyst layer (CL) ice volume fraction, and temperature for the edge cell (cell-1) and the central cell (cell-15) at initial temperatures of -12 °C and -14 °C. The distinct characteristics and their synergistic mechanisms are analyzed as follows.

As shown in Figure 3 (a), the voltage evolutions of cell-1 and cell-15 at -12 °C exhibit a three-stage behavior characterized by "synchronous decline – differentiated recovery – convergence." During the initial cold-start stage (0–10 s), severe activation and ohmic polarization losses under subzero conditions lead to a rapid and simultaneous voltage drop in both cells, with minimum values approaching 0.4 V. In the subsequent stage (10–25 s), inter-cell differences gradually emerge. Owing to its central position within the stack and relatively favorable thermal environment, cell-15 experiences a faster temperature rise, resulting in progressive mitigation of polarization losses and steady voltage recovery. In contrast, cell-1, strongly affected by heat dissipation from the metallic end plate, exhibits a significantly delayed temperature increase. Continuous ice accumulation in its cathode CL further aggravates mass transport resistance, leading to slower alleviation of polarization losses and a continued gradual voltage decline.

At t = 25 s, the linear loading phase ends, and the current density reaches 0.5 A·cm^{-2}, entering the constant-current stage. The enhanced reaction heat generation markedly accelerates the temperature rise, producing an inflection point in both voltage curves. Thereafter, the recovery rates of cell-1 and cell-15 gradually converge, and the voltage difference progressively decreases, ultimately stabilizing at approximately 0.5 V. Throughout the entire process, cell-1 does not experience persistent low voltage or voltage collapse, which serves as a critical prerequisite for successful stack cold start.

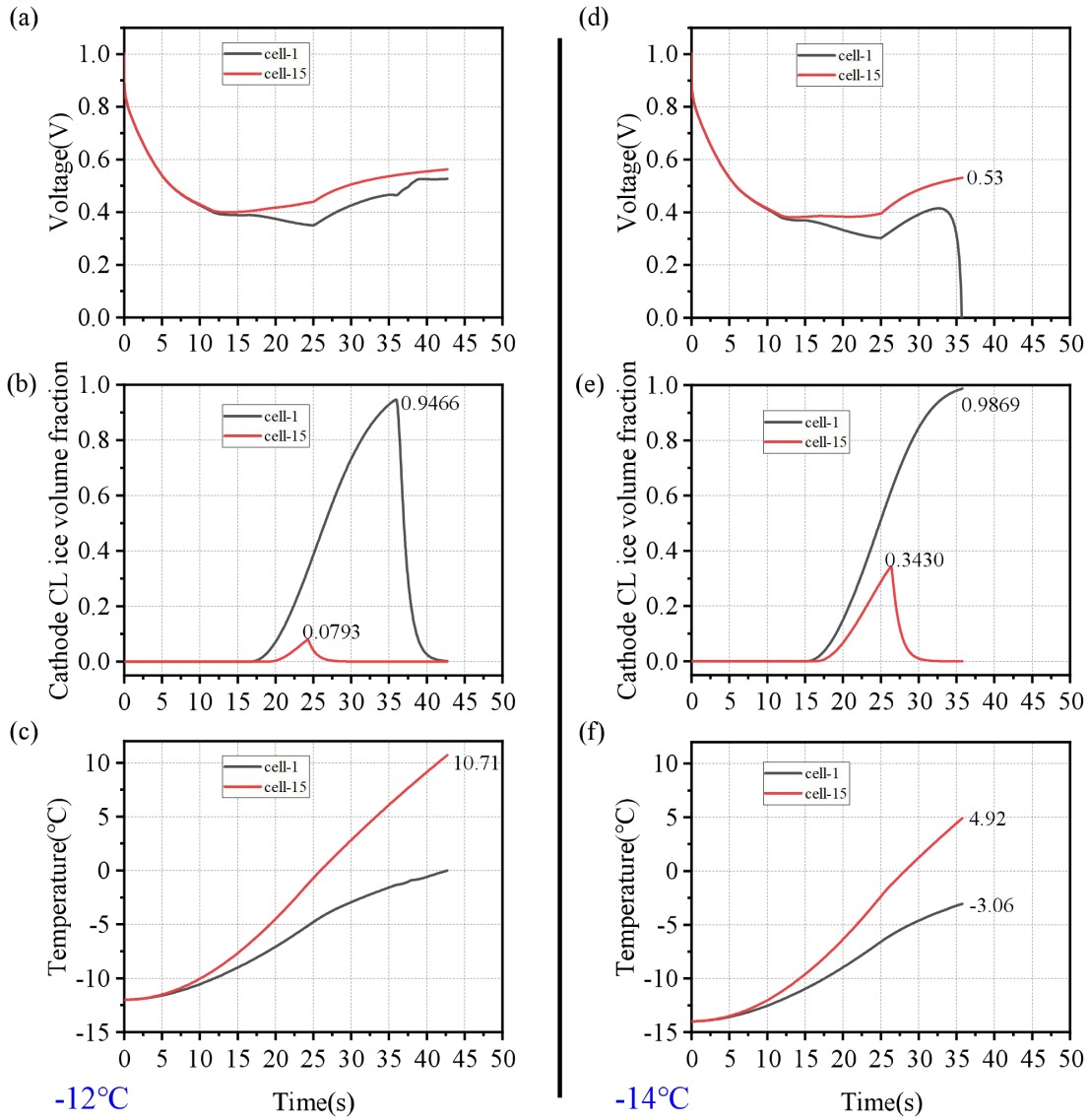

Figure 3 Voltage, Cathode CL Ice Volume Fraction, and Temperature Variations over Time for Cell-1 and Cell-15 at Start-Up Temperatures of -12°C and -14°C

Figure 3 (b) illustrates the pronounced difference in the cathode CL ice volume fraction between the two representative cells. For cell-1, the ice volume fraction reaches a peak of 0.9466 at approximately 35 s, which is substantially higher than that of cell-15 and occurs noticeably later. After the temperature surpasses the freezing point, the ice fraction of cell-1 rapidly declines to zero. In contrast, cell-15 exhibits only a modest peak value of 0.0793 at around 25 s, followed by rapid attenuation. This disparity primarily arises from the non-uniform temperature recovery rates among cells. The edge cell (cell-1) remains below the freezing point for an extended period, causing electrochemically generated water to continuously accumulate in the form of ice crystals, thereby resulting in a higher and delayed peak. Conversely, the central cell (cell-15) heats up more rapidly, exceeds 0 °C at an earlier stage, and produces water predominantly in liquid form, leading to only a limited and transient ice accumulation.

The single-cell temperature evolutions shown in Figure 3 (c) further corroborate this interpretation. Throughout the cold-start process, the temperature rise rate of cell-15 remains consistently higher than that of cell-1. When cell-1 recovers to 0 °C at approximately 42 s, the temperature of cell-15 has already reached 10.71 °C, yielding a temperature difference exceeding 10 °C. This pronounced thermal gradient directly governs the melting behavior. Cell-15 achieves ice melting at an earlier stage, while cell-1, despite delayed heating, is still able to surpass the freezing point at a critical time, enabling rapid melting of its accumulated ice. This prevents sustained blockage of the cathode mass transport pathways and ensures successful completion of the cold start.

Compared with the -12 °C case, the early-stage evolution at -14 °C is generally similar, but substantial differences emerge at later stages. During the initial period, the voltages of both cells decrease synchronously due to intensified polarization losses under lower temperature, with overall voltage levels slightly lower than those at -12 °C. As the process proceeds, cell-15 gradually recovers with increasing temperature and stabilizes at approximately 0.53 V. In contrast, the voltage of cell-1 exhibits delayed recovery and abruptly drops to zero after approximately 35 s, indicating voltage collapse. This behavior signifies severe mass transport failure in the edge cell. Although the central cell remains operational, the overall stack can no longer sustain operation, ultimately resulting in cold-start failure.

The evolution of the cathode CL ice volume fraction further reveals the root cause of failure. For cell-1, the ice fraction reaches 0.9869 at around 35 s and remains at a persistently high level without decline. By comparison, cell-15 exhibits a peak value of only 0.3430, which rapidly decays to zero after approximately 25 s. The fundamental reason lies in the asymmetric temperature recovery: cell-15 heats up rapidly and surpasses the freezing point at an earlier stage, allowing ice melting to occur. In contrast, cell-1, continuously subjected to strong heat dissipation from the end plate, remains below the freezing point, causing continuous ice accumulation from electrochemically generated water and ultimately leading to complete blockage of the cathode mass transport channels.

The temperature evolution clearly establishes the criterion for cold-start failure. At 35 s, the temperature of cell-15 has risen to 4.92 °C, well above the freezing point, whereas that of cell-1 remains at -3.06 °C and never exceeds the freezing threshold. This condition—where some cells satisfy the thermal requirement while others do not—constitutes the fundamental cause of failure. Successful stack cold start requires all single cells to escape subfreezing and ice-accumulation conditions; recovery of central cells alone cannot compensate for the failure of edge cells.

4 CONCLUSION

This study systematically investigated the cold-start behavior of PEMFCs under different initial temperature conditions and identified a distinct temperature boundary (approximately -12 °C to -14 °C) under a unified linear 25 s loading strategy. The results demonstrate that cold-start success or failure is not simply governed by the overall heat generation capacity of the stack, but is predominantly controlled by the local thermal constraints of the edge cells. Owing to the heat dissipation effect of the end plates, edge cells exhibit pronounced thermal lag under subzero conditions. Whether their temperature can surpass the freezing point within a critical time window directly determines the evolution of the ice phase in the cathode catalyst layer and the recoverability of mass transport pathways.

When the edge cells successfully exceed the freezing threshold, the system undergoes a dynamic transition from localized disparity to overall coordination, gradually establishing a stable operating state. Conversely, persistent ice accumulation triggers mass transport failure and voltage collapse, ultimately leading to cold-start failure. Therefore, the minimum temperature response of the edge cells can be regarded as the dominant controlling variable for cold-start stability, and the temperature interval of -12 °C to -14 °C constitutes the success boundary under the present loading protocol.

From the perspective of cell-to-cell consistency, this study elucidates the formation mechanism of the cold-start limit and provides a theoretical basis for optimizing low-temperature startup strategies and defining boundary conditions for enhanced operational reliability.

COMPETING INTERESTS

The authors have no relevant financial or non-financial interests to disclose.

REFERENCES

[1] Luo Y, Jiao K. Cold start of proton exchange membrane fuel cell. Progress in Energy and Combustion Science, 2018, 64: 29–61. https://doi.org/10.1016/j.pecs.2017.10.003.

[2] Zang L, Zhu X, Hao L. Study of three factors for commercial-size PEM fuel cell stack cold start: Manifold, endplate, and assisted heating. Fuel, 2024, 373: 132335. https://doi.org/10.1016/j.fuel.2024.132335.

[3] Zhang C, Chen J, Luo M, et al. Modelling, validation and analysis of preheating strategy of fuel cell vehicle during Subzero cold start. International Journal of Heat and Mass Transfer, 2024, 220: 124889. https://doi.org/10.1016/j.ijheatmasstransfer.2023.124889.

[4] Lin R, Zhu Y, Ni M, et al. Consistency analysis of polymer electrolyte membrane fuel cell stack during cold start. Applied Energy, 2019, 241: 420–32. https://doi.org/10.1016/j.apenergy.2019.03.091.

[5] Takahashi T, Kokubo Y, Murata K, et al. Cold start cycling durability of fuel cell stacks for commercial automotive applications. International Journal of Hydrogen Energy, 2022, 47: 41111–23. https://doi.org/10.1016/j.ijhydene.2022.09.172.

[6] Huo S, Jiao K, Park JW. On the water transport behavior and phase transition mechanisms in cold start operation of PEM fuel cell. Applied Energy, 2019, 233–234: 776–88. https://doi.org/10.1016/j.apenergy.2018.10.068.

[7] Liu J, Chen H, Zhang T. Analysis of cold start characteristics in a PEMFC stack with different current loading modes. International Journal of Hydrogen Energy, 2024, 51: 1456–76. https://doi.org/10.1016/j.ijhydene.2023.06.303.

[8] Alemohammad S, Ahmadi P. Investigation of modeling challenges of PEM fuel cells cold start operation. International Journal of Hydrogen Energy, 2024, 52: 1192–212. https://doi.org/10.1016/j.ijhydene.2023.10.188.

[9] Shi L, Du C, Liu Z, et al. Identification of the cold start boundaries of proton exchange membrane fuel cells based on one dimensional multi-phase model. Renewable Energy, 2025, 240: 122222. https://doi.org/10.1016/j.renene.2024.122222.

[10] Seleem SI, Hasanien HM, El-Fergany AA. Equilibrium optimizer for parameter extraction of a fuel cell dynamic model. Renewable Energy, 2021, 169: 117–28. https://doi.org/10.1016/j.renene.2020.12.131.